Fabrication and antimicrobial performance evaluation of ZnO@HA bioceramic and ZnO@PVP polymer nanocomposites

Hussein Mohamed Sadeq* - Ph.D Al-Furat Al-Awsat Technical University, Polytechnic College-Karbala, Mechanical Technologies Engineering Department, Iraq - - - - boshrags.bg@gmail.com
---
- - - -
Hamzah Zahraa Saad - phd 1Al-Furat Al-Awsat Technical University, Polytechnic College-Karbala, Mechanical Technologies Engineering Department, Iraq - - - - zahraa.saad@s.uokerbala.edu.iq
---
- - - -
Layth Hayder Hameed Kazem Al_Tmamimi - phd Al-Furat Al-Awsat Technical University, Polytechnic College-Karbala, Mechanical Technologies Engineering Department, Iraq - - - - laith.hamid.ikr14@atu.edu.iq
---
* - - -
Mohammed Ridha Shaeed Janabi - phd 2University of Babylon, Science for women, Laser Physics, Babylon, Iraq - - - - wsci.mohammed.aljanabi@uobabylon.edu.iq
---
- - - -
Tabarek Falah Deindee - phd University of Babylon, College of Science, Department of Physics, Babylon, Iraq - - - - sci.tabarek.salim@uobabylon.edu.iq
---

In Press

[Downloaded from ijmse.iust.ac.ir on 2026-11-02]

[DOI: 10.22068/ijmse.4598]

Abstract

The spread of pathogenic microorganisms in the food, pharmaceutical and active packaging industries has created serious health and economic challenges. Among them, zinc oxide (ZnO) nanoparticles have attracted attention as effective antimicrobial agents; however, particle aggregation and functional limitations limit their individual application. The aim of this study was to synthesize ZnO

nanoparticles and prepare ZnO@HA and ZnO@PVP nanocomposites and comprehensively evaluate their structural, optical and antibacterial properties. ZnO nanoparticles were synthesized by sol-gel method and nanocomposites were prepared by solution mixing and polymer coating methods, respectively. The X-ray diffraction results confirmed the formation of hexagonal wurtzite structure of ZnO with characteristic peaks at 31.8, 34.4 and 36.3 degrees, indicating the appropriate phase purity of the samples. The FTIR spectra showed the presence of a characteristic Zn-O band around 500 cm^{-1} and in the composite samples the presence of phosphate groups related to HA and organic PVP groups was clearly observed, indicating the success of the phase interaction. FESEM images showed that pure ZnO has a nanoscale aggregated granular morphology; while the addition of HA caused a decrease in particle size and the formation of a dense and uniform nanostructured network. In contrast, in the ZnO@PVP sample, spherical structures were observed on the micrometer scale, indicating an increase in particle aggregation. Optical studies have shown that a characteristic absorption peak of ZnO appears at around 375 nm. The energy gap values for pure ZnO, ZnO@HA, and ZnO@PVP were 3.13, 1.75, and 4.13 eV, respectively. The antibacterial test against "*Escherichia coli*" showed that ZnO@HA nanocomposite is a promising candidate for antimicrobial applications, active packaging, and biomedical systems due to its stable nanometer size, reduced energy gap, and enhanced antibacterial activity.

Keywords: ZnO@HA and ZnO@PVP nanocomposite, antibacterial activity, sol-gel method, physical and optical characterizations

Introduction

Improving the standard of living and life expectancy is closely linked to health and adherence to public health principles, which has placed immense responsibility on various industries, such as the food, active packaging, and pharmaceutical sectors

[Downloaded from ijmse.iust.ac.ir on 2026-11-02]

[DOI: 10.22068/ijmse.4598]

In Press

[1]. The growth and spread of harmful pathogenic microorganisms not only render products unacceptable for consumers but also endanger human lives [1-3]. Hospital infections, foodborne pathogens, skin infections, and microbial-induced contamination impose huge economic losses and significantly increase mortality [2-5]. Over the past decades, numerous traditional efforts, including physical and chemical methods, have been made to eliminate these microbial organisms [6]. However, evolving microbial resistance has caused double concern for societies, threatening modern medicine and environmental safety [7, 8]. With the emergence of nanotechnology, highly effective strategies have been proposed to combat these biological agents. Nanomaterials, cause to their high surface-to-volume ratio, small size, high penetration capacity, and several simultaneous mechanisms of activity, provide vastly excellent antimicrobial properties contrast to their bulk counterparts [9, 10].

Among different engineered nanostructures, zinc oxide (ZnO) nanoparticles have emerged as a highly appropriate choice for antimicrobial applications. They present significant advantages due to their broad spectrum of activity, relatively low cytotoxicity, and cost-effectiveness [11-13]. ZnO can inactivate and destroy the functional compounds of microbes by producing reactive oxygen species (ROS) such as free radicals, releasing zinc ions that disrupt cellular systems, and physically interacting with cells [14-16]. These photocatalytic nanoparticles have found wide applications in active food packaging, wound dressings, and antimicrobial formulations [17-21]. However, the effective use of pure, zero-dimensional ZnO nanoparticles is severely restricted by their functional limitations. Pure ZnO has a powerful thermodynamic trend for particle agglomeration and aggregation, which decreases its active surface area and overall effect [22, 23]. Moreover, because of its noticeable sensitivity to pH, unshielded dissolution in an acidic environment not

[Downloaded from ijmse.iust.ac.ir on 2026-11-02]

[DOI: 10.22068/ijmse.4598]

In Press

only reduces its antimicrobial properties but also strongly affects user safety and toxicity [24]. Thus, careful design and engineering through blending, combining, and composite forming with suitable support matrixes is a critical approach to prevent aggregation and create strong hybrid properties.

The choice of the matrix plays an essential role in dictating the final characteristics of the nanocomposite [25]. Hydroxyapatite (HA) is a highly biocompatible and bioactive inorganic bioceramic that finds wide applications in the biomedical and packaging industries [26]. HA can provide a long-term, chemically stable inorganic skeleton, which is different from organic polymers, and can prevent nanoparticle agglomeration and improve antibacterial activity and stability [26, 27]. In contrast, organic polymers are extremely outstanding in the field of composites and are often selected as matrixes cause to their structural organization [28]. In general, polymers are lightweight, processable, and show a special flexibility along with notable chemical resistance [29]. Polyvinylpyrrolidone (PVP) is a first example of such an organic polymer. When ZnO nanoparticles are blend with an organic matrix such as PVP, the flexible polymer chains give steric hindrance to prevent the agglomeration of nanoparticles, reduce their toxicity, and facilitate processability [23, 30]. Comparing these two distinct materials—a rigid inorganic bioceramic (HA) and a flexible organic polymer (PVP)—is vital to understand how different matrix chemistries influence phase interaction and nanoparticle response.

Therefore, this article aims to investigate the matrix-dependent effects of polyvinylpyrrolidone (PVP) and hydroxyapatite (HA) on the structural, optical, and antibacterial characteristics of ZnO nanoparticles. PVP and HA were explicitly choosing as representative organic polymeric and inorganic ceramic matrixes, respectively, in order to scrutinize how differences in matrix chemistry could affect the morphological evolution and properties of ZnO. Through a general evaluation of

[Downloaded from ijmse.iust.ac.ir on 2026-11-02]

[DOI: 10.22068/ijmse.4598]

In Press

pure ZnO, ZnO@HA, and ZnO@PVP nanocomposites, this study attempts to address the functional limitations of pure ZnO and highlight the most promising chose for advanced antimicrobial applications, active packaging, and biomedical systems.

2. Materials and Methods

2-1. Materials

Zinc acetate dihydrate ($Zn(CH_3COO)_2 \cdot 2H_2O$) and sodium hydroxide (NaOH) were respectively adopted as zinc precursor and precipitating agent. The PVP and HA were employed as organic polymeric and inorganic ceramic matrices, respectively, for the preparation of the nanocomposites. Absolute ethanol and deionized water were hired as solvents. All materials were of laboratory quality and used without further purification.

2-2. Synthesis Methods

2-2-1. Synthesis of ZnO nanoparticles by the sol-gel method

ZnO nanoparticles were prepared by a simple sol-gel method according to the method reported in research studies [31, 32]. First, a 0.1 M solution of zinc acetate dihydrate was prepared in 100 mL of ethanol/deionized water and continued to be stirred under magnetic stirring at room temperature until a clear solution was formed. Then, a 1 M NaOH solution was added dropwise to the solution under vigorous stirring to establish an OH^-/Zn^{2+} molar ratio of about 2. With the increase in hydroxide ions, the hydrolysis process began and a white sol was formed. The reaction mixture was kept at 50-60°C for 1 h to complete the gelation process. According to reports, in this temperature range, the reaction of zinc acetate and NaOH leads to the formation of the hydroxide precursor and then nanocrystalline ZnO. The resulting precipitate was collected by centrifugation and washed several

[Downloaded from ijmse.iust.ac.ir on 2026-11-02]

[DOI: 10.22068/ijmse.4598]

In Press

times with deionized water and ethanol. The sample was dried at 80 °C for 12 hours and then calcined at 400 °C for 2 hours to form ZnO nanoparticles.

2-2-2. Synthesis of ZnO@HA nanocomposite by solution mixing method

The ZnO@HA nanocomposite was prepared by a simple chemical mixing method that has been reported in studies of bioceramic composites [27]. First, 0.5 g of synthesized ZnO nanoparticles were sonicated in 100 mL of deionized water for 30 min to obtain uniform dispersion. Separately, the hydroxyapatite powder was dispersed in the same solvent (ZnO:HA weight ratio = 1:1). Then, the HA suspension was slowly added to the ZnO suspension and the mixture was magnetically stirred at 60 °C for 3 h to establish bonding and interaction between the phases. It has been reported that mixing the solution at a mild temperature result in uniform distribution of ZnO in HA. Finally, the product was collected by centrifugation, washed with DI Water and dried at 80 °C for 12 hours to obtain the ZnO@HA nanocomposite.

2-2-3. Synthesis of ZnO@PVP nanocomposite by polymer coating method

The ZnO@PVP nanocomposites were prepared by means of a solution coating method [30]. In this regard, 1 g of PVP polymer was dissolved in 100 mL of ethanol under magnetic stirring at room temperature to form a clear solution. Then, 0.5 g of ZnO nanoparticles were gradually added to the solution. The mixture was sonicated for 1 h and then, magnetically stirred for 4 h to coat the PVP chains on the surface of nanoparticles. Finally, the solvent was evaporated at 70 °C and the product was dried in an oven at 80 °C for 12 h to obtain ZnO@PVP nanocomposite.

2-3. Characterization Methods

XRD, FTIR, FESEM, EDX, Raman, UV–Vis, and agar disk diffusion tests were used to investigate the properties of the samples.

In Press

[Downloaded from ijmse.iust.ac.ir on 2026-11-02]

[DOI: 10.22068/ijmse.4598]

3. Results and discussion

3.1. Characterization analyses

X-ray diffractogram of pure ZnO nanoparticles is available in Figure 1a, which is illustrated in the 2θ ranging from 10 to 80°. Accordingly, several diffraction peaks appear at 31.8, 34.4, 36.3, 47.6, 56.6, 62.9, 66.5, 67.9, 69.1, 72.8, and 77.1°, which respectively corresponds to Miller indices of (100), (002), (101), (102), (110), (103), (200), (112), (201), (004), and (202). In accordance with JCPDS card No. 36-1451, the aforementioned peaks represent hexagonal wurtzite structure of ZnO [33-35].

Compositing ZnO nanoparticles with HA resulted in some changes in their XRD pattern. In this regard, the crystalline planes detected for pure ZnO nanoparticles, including (100), (002), (101), (102), (110), (103), (200), (112), and (201) are also observed for their counterparts composited with HA (Figure 1b). However, compositing process gave rise to decrement in their intensity. The diffraction peaks indicated by asterisk in Figure 1b occur at 2θ positions that coincide exactly with characteristic reflections of hydroxyapatite (Figure 1c), suggesting that they may arise from overlapping diffraction peaks of ZnO and hydroxyapatite, rather than being exclusively attributable to ZnO.

In Press

[Downloaded from ijmse.iust.ac.ir on 2026-11-02]

[DOI: 10.22068/ijmse.4598]

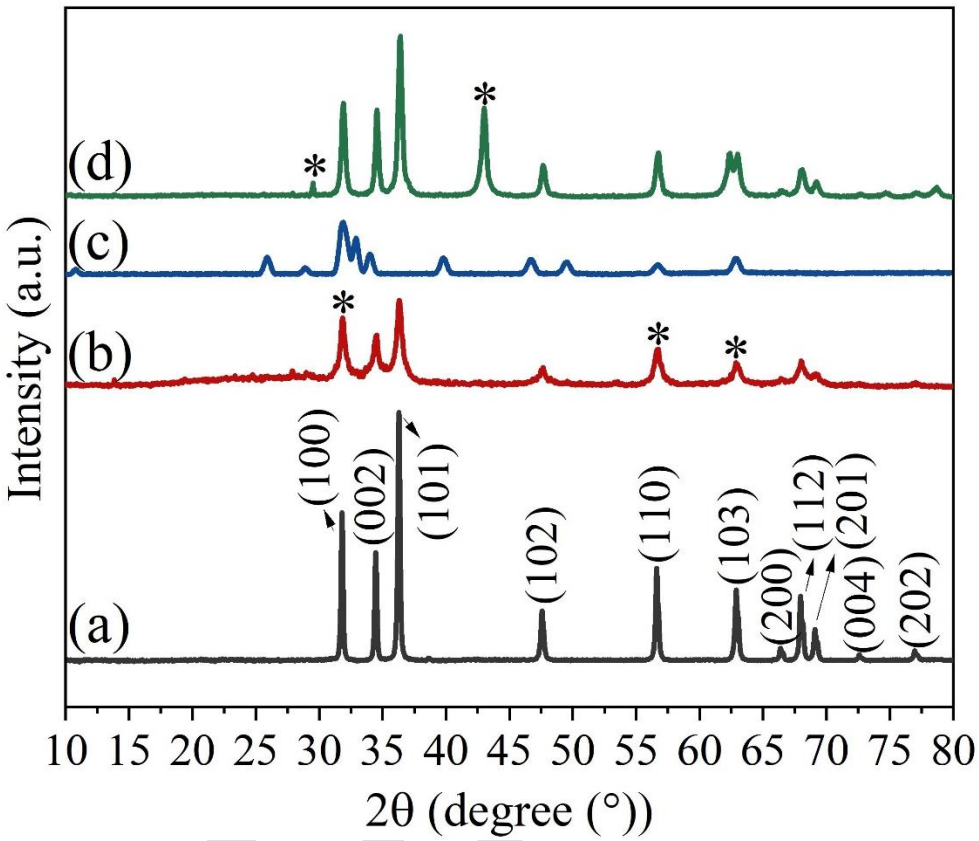


Figure 1. X-ray diffractograms of (a) ZnO, (b) ZnO@HA, (c) pure HA, and (d) ZnO@PVP.

For ZnO@PVP (Figure 1d), in addition to diffraction peaks related to pure ZnO, additional peaks are also evident, which are located at 2θ of 29.5 and 43.0°. Since these reflections could not be assigned to the hexagonal wurtzite ZnO phase or crystalline PVP, they may be associated with trace impurities or the formation of minor secondary phase(s) during the synthesis process. Moreover, some crystalline planes for instance (004) and (202) disappeared from X-ray diffractogram of ZnO@PVP composite.

FTIR spectroscopy was another characterization test adopted for identification of functional groups or chemical bonds within prepared samples. As evidenced from FTIR spectrum of pure ZnO nanoparticles (see Figure 2), a broad absorption band is detectable at 3430 cm^{-1}, which is associated with hydroxyl (O-H) groups present in adsorbed water molecules [36, 37].

[Downloaded from ijmse.iust.ac.ir on 2026-11-02]

[DOI: 10.22068/ijmse.4598]

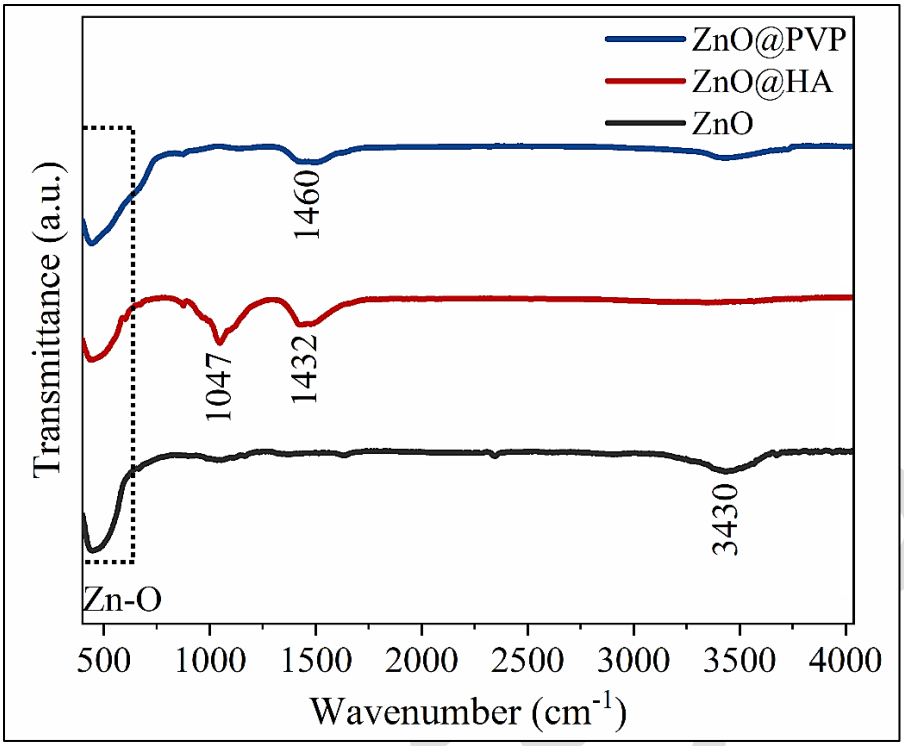


Figure 2. FTIR spectra of pure ZnO nanoparticles and their composites.

In addition, a well-defined peak is found near 500 cm^{-1}. Based on references, metal-oxygen bonds typically appear in the wavenumber from 400 to 800 cm^{-1} [38, 39]. As a consequence, the peak near 500 cm^{-1} pertains to Zn-O bond. In the FTIR spectrum of ZnO@HA composite, in addition to peak demonstrating Zn-O bond, a sharp absorption band is seen at 1047 cm^{-1}, which is ascribed to the stretching vibration of PO_4^{3-} [40]. The peak appears at 1432 cm^{-1} is relevant to asymmetric stretching vibration of carbonate ions (CO_3^{2-}) [40]. Based on references, in hydroxyapatite, phosphate groups sometimes replace by carbonate [26]. In the FTIR spectrum of ZnO@PVP composite, the peak related to Zn-O and also the peak exhibiting C-H group (alkane groups) at 1460 cm^{-1} can be found [41].

[Downloaded from ijmse.iust.ac.ir on 2026-11-02]

[DOI: 10.22068/ijmse.4598]

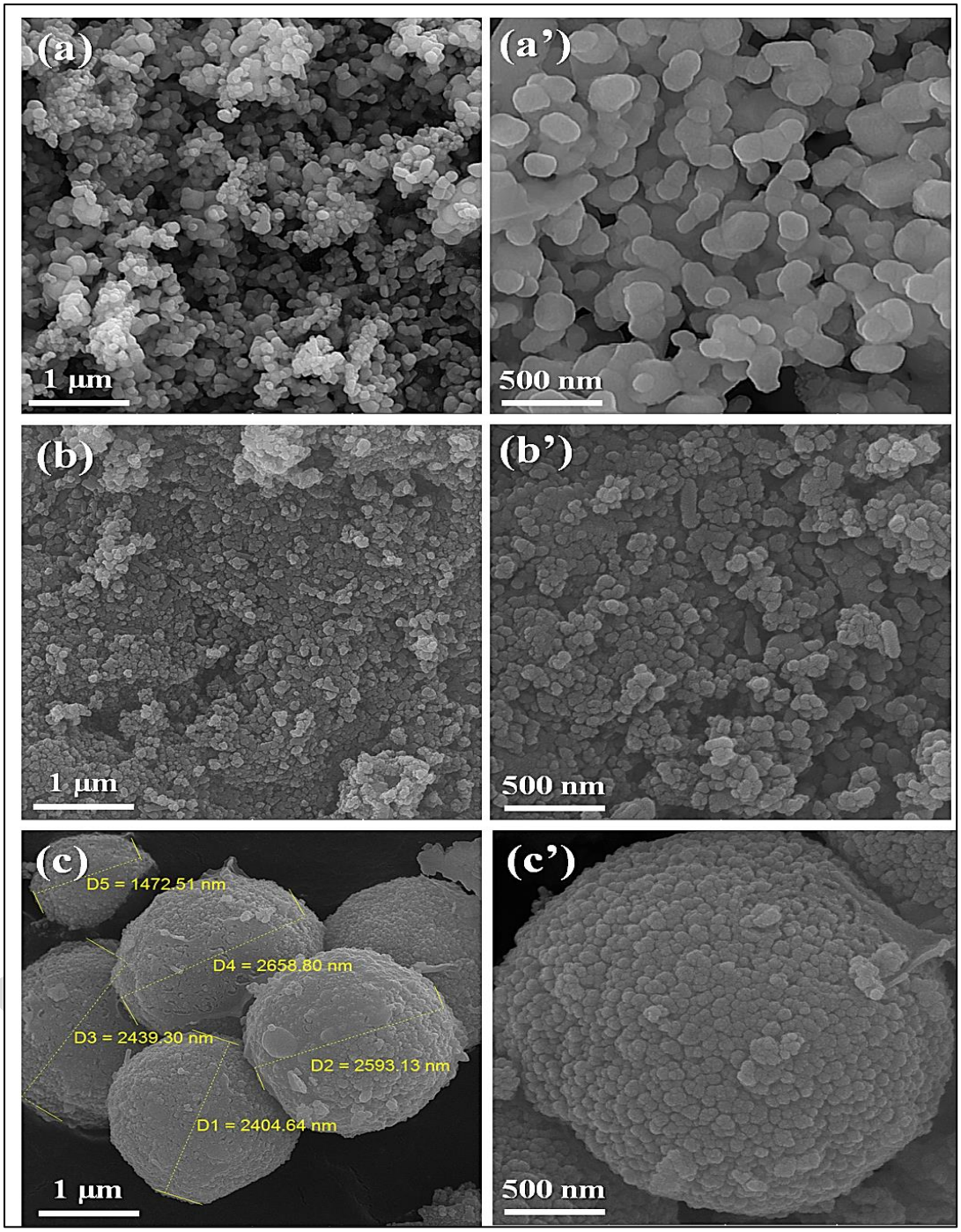


Figure 3. FESEM images of (a,a') pure ZnO, (b,b') ZnO@HA, and (c,c') ZnO@PVP recorded at different magnifications.

Morphology of pure ZnO nanoparticles was examined using FESEM analysis. According to Figure 3a, agglomerated granular-shaped nanostructures of ZnO with well-separated grain boundaries are evident. The dispersed grains show different

[Downloaded from ijmse.iust.ac.ir on 2026-11-02]

[DOI: 10.22068/ijmse.4598]

shape and size (Figure 3a'). Compositing nanostructured ZnO particles with HA gave rise to the change of their morphology. In this regard, a compact network of aggregated granular-shaped nanoparticles can be seen for ZnO@HA composite (Figure 3b). The comparison between Figures 3a' and 3b' reveals that incorporation of ZnO nanoparticles into the HA matrix promoted nanoparticle agglomeration and resulted in the formation of a more compact and interconnected network. In the FESEM image of ZnO@PVP composite, bulky spherical-shaped microstructures (Figure 3c) composed of very small nanoparticles (Figure 3c') are detectable.

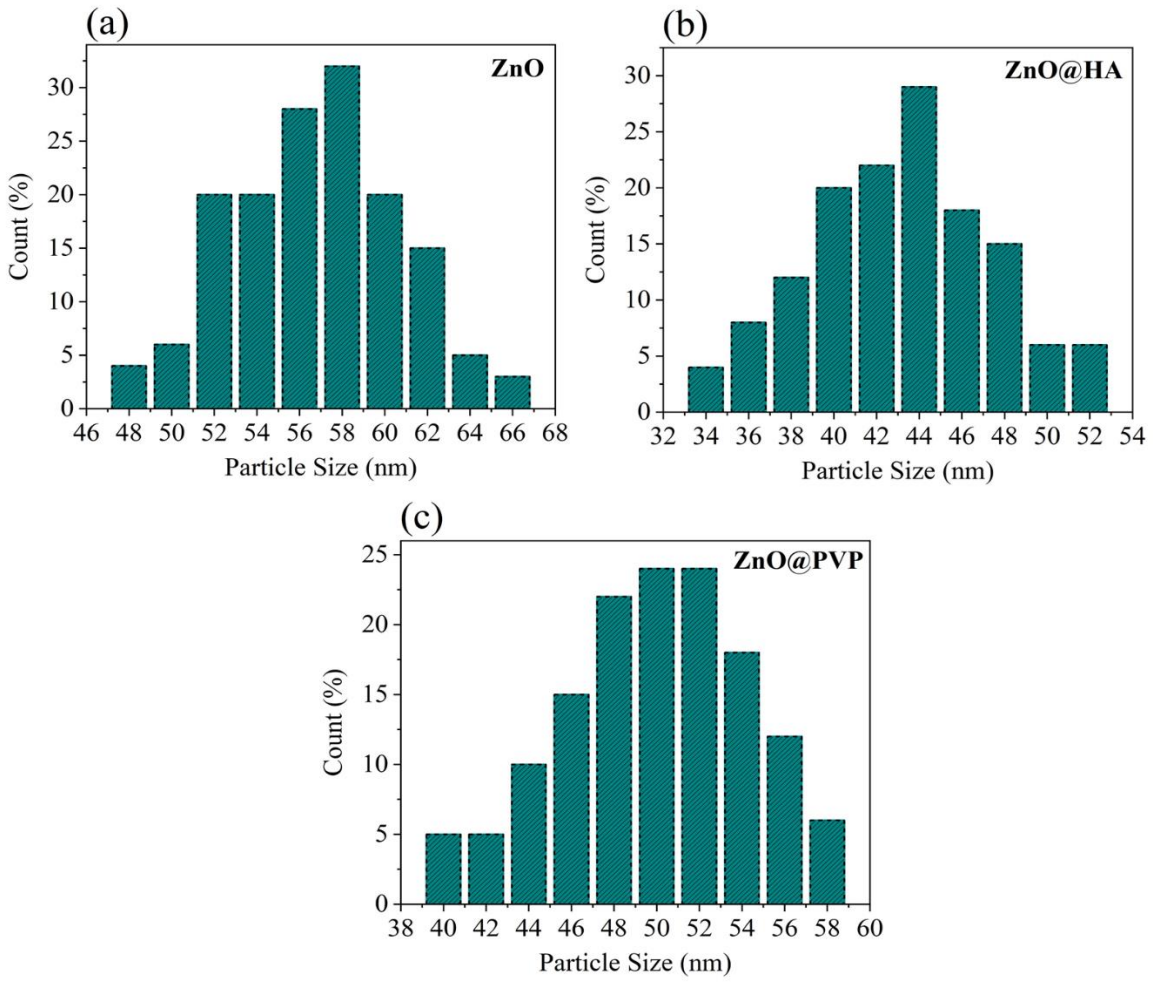


Figure 4. Particle size histograms of ZnO nanoparticles and their nanocomposites obtained from their FESEM images

[Downloaded from ijmse.iust.ac.ir on 2026-11-02]

[DOI: 10.22068/ijmse.4598]

Figure 4 demonstrates particle size histograms of ZnO nanoparticles and their nanocomposites extracted from their FESEM images. In this regard, the majority of ZnO nanoparticles exhibit average size of 58 nm. Obviously, compositing ZnO nanoparticles with each of HA or PVP gave rise to decrement in their particle size where average sizes of 44 and 51 nm were respectively recorded for ZnO@HA and ZnO@PVP nanocomposites.

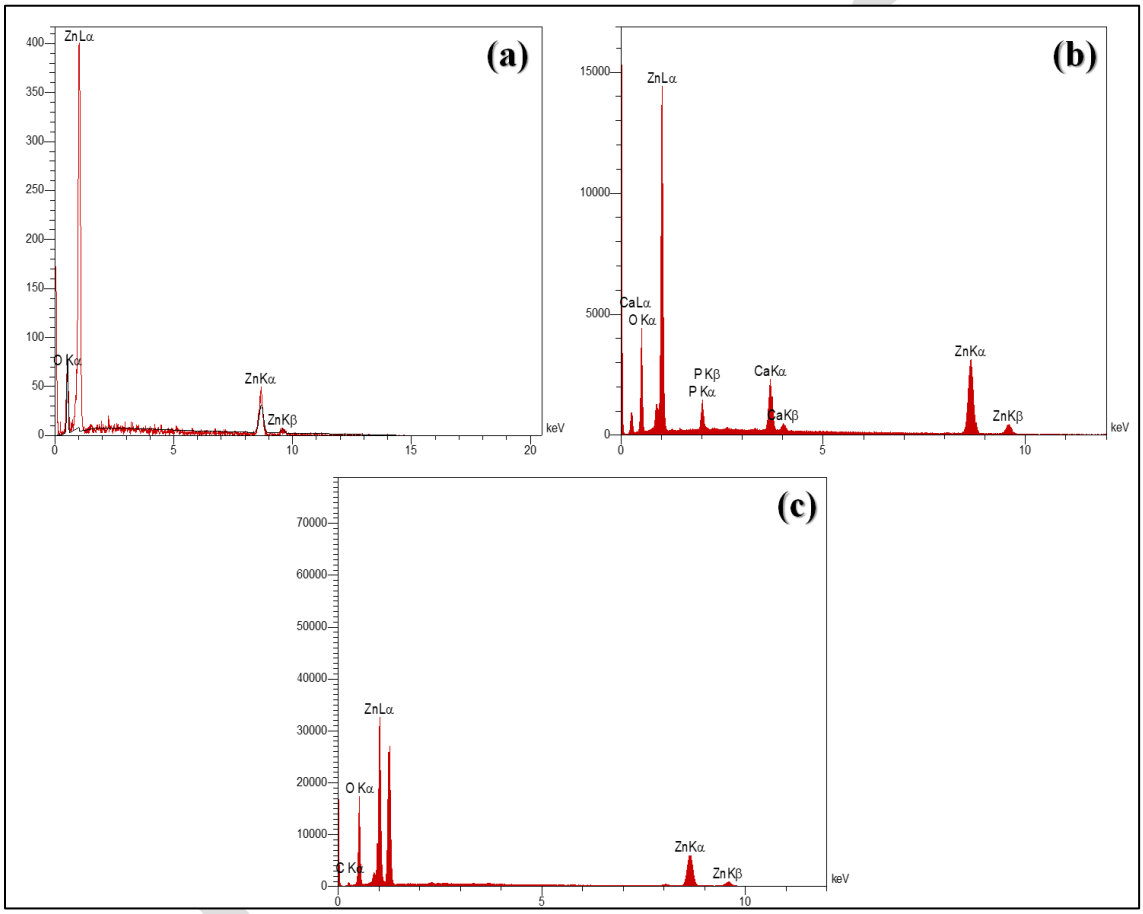


Figure 5. EDXS patterns of (a) pure ZnO, (b) ZnO@HA, and (c) ZnO@PVP.

In addition to FESEM images, EDXS patterns were recorded for ZnO nanoparticles and their nanocomposites. As evidenced from Figure 5a showing EDXS pattern of pure ZnO, the pronounced peak of oxygen (O) element at 0.5 keV and peaks of zinc (Zn) element at 1.0, 8.5, and 9.5 keV are evident. In the EDXS pattern of ZnO@HA composite (Figure 5b), the peaks of O and Zn relevant to ZnO and the peaks of O,

[Downloaded from ijmse.iust.ac.ir on 2026-11-02]

[DOI: 10.22068/ijmse.4598]

calcium (Ca), phosphorus (P) pertinent to hydroxyapatite are found. Figure 5c reveals EDXS pattern of ZnO@PVP. Accordingly, and in addition to peaks originating from ZnO, the peaks demonstrating PVP polymer, including carbon (C) and O, are noticeable. The quantitative results obtained from EDXS patterns of samples are listed in Tables 1 to 3.

Table 1. The results obtained from EDXS pattern of pure ZnO.

Element	Line	Intensity	Error	K	Kr	W%	A%
O	Ka	64.3	4.3992	0.1578	0.1281	25.38	58.16
Zn	Ka	72.3	1.0422	0.8422	0.6834	74.62	41.84
				1.0000	0.8115	100.00	100.00

Table 2. The results obtained from EDXS pattern of ZnO@HA composite.

Element	Line	Intensity	Error	K	Kr	W%	A%
O	Ka	242.6	175.3219	0.1852	0.1226	36.81	64.59
P	Ka	118.7	85.3768	0.0994	0.0658	8.97	8.13
Ca	Ka	228.7	39.8769	0.2105	0.1394	14.72	10.31
Zn	Ka	433.0	0.6664	0.5050	0.3343	39.49	16.96
				1.0000	0.6621	100.00	100.00

Table 3. The results obtained from EDXS pattern of ZnO@PVP composite.

Element	Line	Intensity	Error	K	Kr	W%	A%
C	Ka	42.6	121.4362	0.0142	0.0083	4.35	10.11
O	Ka	959.2	188.3516	0.3242	0.1888	37.26	64.97
Zn	La	1897.5	419.3359	0.6617	0.3853	58.38	24.91
				1.0000	0.5823	100.00	100.00

Raman spectrum of uncomposited ZnO nanoparticles is available in Figure 6. Accordingly, the sharp Raman peak detectable at 434 cm^{-1} shows E_2 (High) mode, which originates from the Raman active optical phonon mode related to the wurtzite structure of ZnO nanoparticles. Another peak is found at 585 cm^{-1}, which

[Downloaded from ijmse.iust.ac.ir on 2026-11-02]

[DOI: 10.22068/ijmse.4598]

In Press

demonstrates vibration mode of E_1 (LO) ZnO. The aforementioned peaks reveal that multiphoton resonances are available in ZnO nanoparticles with a crystalline structure [42, 43]. In addition to Raman peaks related to ZnO, two peaks are observed at 1372 and 1603 cm^{-1}. The former, based on literature, could be ascribed to the carbonate species associated with the interaction between the atmospheric CO_2 molecules with ZnO [56]. The latter is assigned to the H–O–H bending (ν_2) mode of water molecules [42, 43].

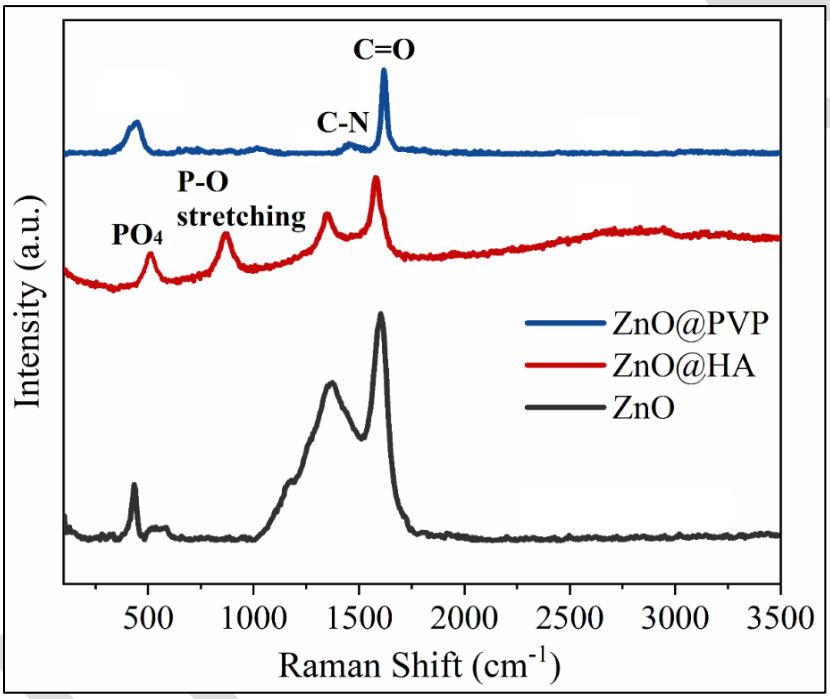


Figure 6. Raman spectra of pure nanostructured ZnO particles and their fabricated composites.

In the Raman spectrum of ZnO composited with HA, in addition to peaks related to carbonate species and water molecules respectively at 1372 and 1603 cm^{-1}, another peak appears near 1000 cm^{-1}, which pertains to symmetric stretching mode of P-O-P in PO_4^{3-} ion [27, 44]. Another peak found at about 500 cm^{-1}, which is related to PO_4^{3-} in a triply degenerate bending mode [27]. Raman spectrum of ZnO@PVP composite is shown in Figure 6. Accordingly, the peak showing E_2 (High) mode of ZnO is evident near 500 cm^{-1}. Besides, two peaks are detected at about 1500 and

[Downloaded from ijmse.iust.ac.ir on 2026-11-02]

[DOI: 10.22068/ijmse.4598]

1600 cm^{-1}, which respectively exhibit vibrational mode of C-N and C=O bonds within PVP [30].

3.2. Optical properties investigation

In order to examine optical properties of prepared samples, their absorbance UV-Visible spectra were recorded. In accordance with UV-Visible spectrum of pure ZnO nanoparticles (Figure 7), a well-defined peak is observed at about 375 nm, which is characteristic of zinc oxide [45, 46]. Compositing ZnO nanoparticles with HA gave rise to some changes in their UV-Visible spectrum. In this regard, the peak found at 375 nm is also detected in the UV-Visible spectrum of ZnO@HA composite whose intensity is less than the one observed for pure ZnO. Like other samples, the characteristic peak of ZnO at 375 nm also appears in the UV-Visible spectrum of ZnO@PVP composite, which shows the least intensity compared to pure ZnO and also ZnO@HA composite.

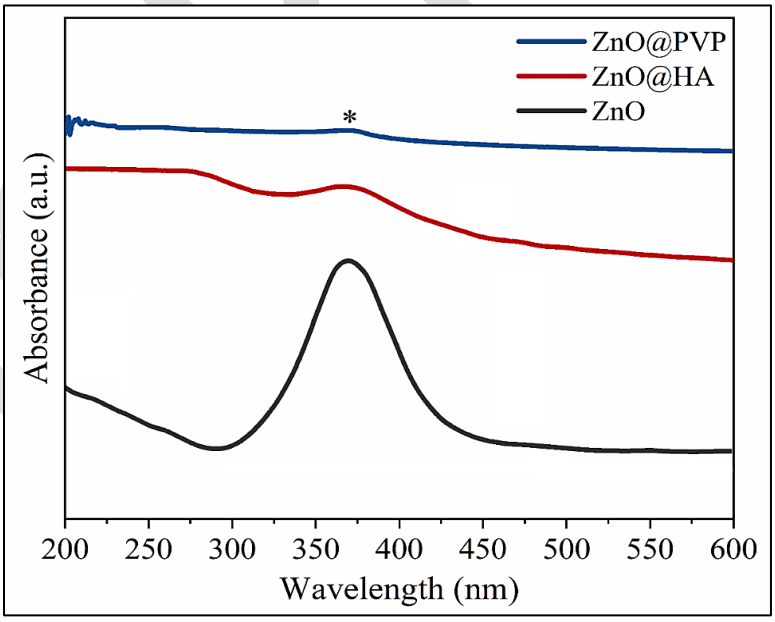


Figure 7. UV-Visible absorbance spectra of pure nanostructured ZnO particles and their fabricated composites.

[Downloaded from ijmse.iust.ac.ir on 2026-11-02]

[DOI: 10.22068/ijmse.4598]

The energy band gap (E_g) of pure ZnO nanoparticles and the ones composited with each of HA or PVP was calculated through plotting their Tauc's plots (Figure 8). In Figure 8, α indicates the absorption coefficient. Moreover, $h\nu$ exhibits the incident photon energy. By extrapolating x-axis ($h\nu$) versus y-axis $(\alpha h\nu)^2$ to zero, the E_g value is obtained [47, 48]. The energy band gap calculated for ZnO, ZnO@HA, and ZnO@PVP respectively is 3.13, 1.75, and 4.13 eV. Unlike ZnO@PVP, ZnO@HA composite shows E_g value less than that of pure ZnO.

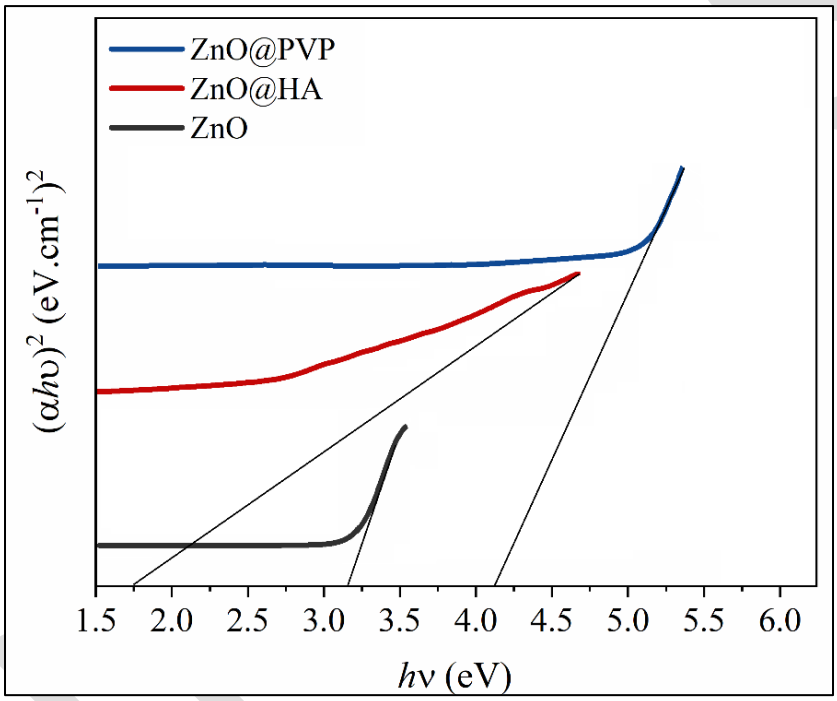


Figure 8. The Tauc's plots of pure ZnO nanoparticles and their fabricated composites.

3.3. Antibacterial activity assessment

Figure 9 represents antibacterial activities examined for pure ZnO nanoparticles and their fabricated composites, including ZnO@HA and ZnO@PVP, against *Escherichia coli* (*E. coli*) bacteria. The measurements were carried out by means of agar-well disk diffusion analysis. The diameter of zone of inhibition appearing around each well was assessed as an appropriate parameter for evaluation of antibacterial activity of samples. As evidenced from Figure 9a exhibiting disk

[Downloaded from ijmse.iust.ac.ir on 2026-11-02]

[DOI: 10.22068/ijmse.4598]

diffusion test conducted for pure ZnO, the gray-color inhibition zone is clearly seen, which testifies antibacterial activity of this sample.

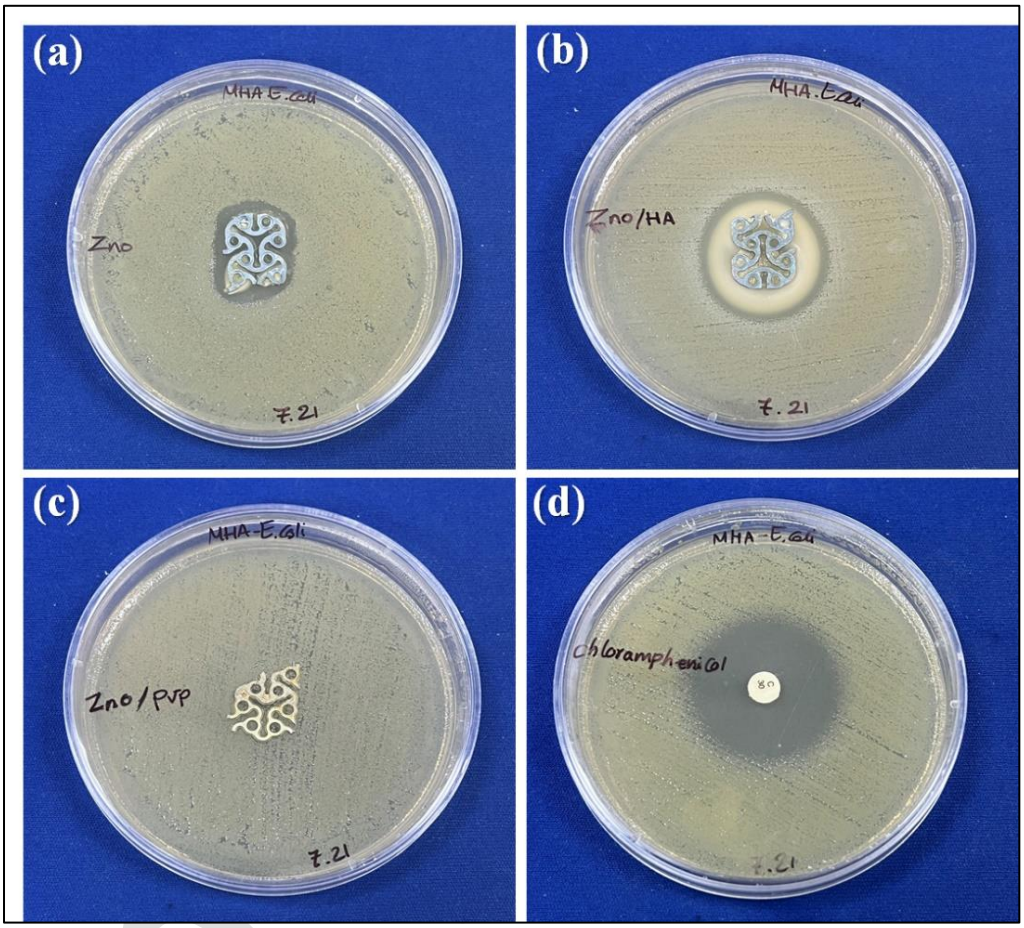


Figure 9. Antibacterial activities measured for (a) pure ZnO, (b) ZnO@HA, (c) ZnO@PVP, and (d) chloramphenicol (positive control) against *E. coli* bacteria using disk-diffusion test.

Compositing ZnO nanoparticles with HA resulted in enhancement in their antibacterial activity. In this regard, the inhibition zone is obviously detectable (Figure 9b) whose diameter is more than the one seen for pure ZnO, which implies higher antibacterial activity of ZnO@HA composite. The comparison between Figures 9b and 9d reveals that antibacterial activity of ZnO@HA composite is comparable with chloramphenicol as a commercial antibiotic. Unlike ZnO and ZnO@HA, no inhibition zone appears for ZnO@PVP (Figures 9c), meaning that it

[Downloaded from ijmse.iust.ac.ir on 2026-11-02]

[DOI: 10.22068/ijmse.4598]

lacks of antibacterial activity. Based on references, antibacterial activity of ZnO particles relies on their size [49]. As evidenced from FESEM images of ZnO@PVP composite, it appeared as micro-sized particles. Micro-sized particles typically show smaller surface areas compared to their counterparts with nanoscale size, which is a weakness since it diminishes antibacterial activity [12]. On the other hand, compositing ZnO nanosized particles with HA reduced their size, which improved their antibacterial activity.

4. Conclusions

In this study, pure ZnO nanoparticles and their composites, including ZnO@HA and ZnO@PVP, were synthesized in order to scrutinize their antibacterial activities. Diffraction peaks showing hexagonal wurtzite structure of ZnO were detected in the XRD patterns of all synthesized composites. Besides, the presence of absorption band related to Zn-O bond in the FTIR spectra of composites was another evidence for the presence of ZnO in their structures. FESEM images manifested that unlike HA whose compositing with ZnO generated nanostructured particles, PVP polymer produced micro-sized particles. Raman spectroscopy was another characterization test confirming fabrication of composites where the peaks showing ZnO, HA, and PVP were detected.

The size of particles of composites significantly affected their antibacterial activities. In this regard, the diameter of zone of inhibition demonstrated by nanostructured ZnO@HA composite was higher than the one seen for pure ZnO. On the other hand, no inhibition zone was detected for ZnO@PVP. The results obtained from this research exhibit that ZnO@HA composite could act as antibacterial agent comparable to chloramphenicol antibiotic.

In Press

[Downloaded from ijmse.iust.ac.ir on 2026-11-02]

[DOI: 10.22068/ijmse.4598]

References

[1] Seema Rawat, *Food Spoilage: Microorganisms and their prevention. Pelagia Research Library Asian Journal of Plant Science and Research, 2015, 5.4, 47–56*. 2015.

[2] Peleg, Anton Y., and David C. Hooper. "Hospital-acquired infections due to gram-negative bacteria." *New England Journal of Medicine*, 2010, 362.19, 1804-1813.

[3] Bintsis, Thomas. "Foodborne pathogens." *AIMS microbiology, 2017,* 3.3, 529.

[4] Chiller, Katarina, Bryan A. Selkin, and George J. Murakawa. "Skin microflora and bacterial infections of the skin." *Journal of Investigative dermatology Symposium proceedings*, 2001, 6.3.

[5] Kchaou, Mohamed, et al. "Surface disinfection to protect against microorganisms: Overview of traditional methods and issues of emergent nanotechnologies." *Applied Sciences, 2020,* 10.17, 6040.

[6] Kchaou, M., et al., *Surface disinfection to protect against microorganisms: Overview of traditional methods and issues of emergent nanotechnologies.* Applied Sciences, 2020, 10.17, 6040.

[7] Wartu, J. R., Butt, A. Q., Suleiman, U., Adeke, M., Tayaza, F. B., Musa, B. J., & Baba, J. "Multidrug resistance by microorganisms: A review.", 2019, 49-56.

[8] Martinez, Jose Luis, *Environmental pollution by antibiotics and by antibiotic resistance determinants.* Environmental pollution, 2009, 157,11,2893-2902.

[9] Yilmaz, Yusuf. "Postbiotics as Antiinflammatory and Immune-Modulating Bioactive Compounds in Metabolic Dysfunction-Associated Steatotic Liver Disease." *Molecular nutrition & food research, 2024,* 68.23, 2400754.

[10] Aguda, O. and A. Lateef, *Recent advances in functionalization of nanotextiles: A strategy to combat harmful microorganisms and emerging pathogens in the 21st century.* Heliyon, 2022, 8, 6.

[11] Jones, N., Ray, B., Ranjit, K. T., & Manna, A. C. "Antibacterial activity of ZnO nanoparticle suspensions on a broad spectrum of microorganisms." *FEMS microbiology letters, 2008,* 279.1 ,71-76.

[12] Sirelkhatim, A., Mahmud, S., Seeni, A., Kaus, N. H. M., Ann, L. C., Bakhori, S. K. M., ... & Mohamad, D., "*Review on zinc oxide nanoparticles: antibacterial activity and toxicity mechanism."* Nano-micro letters, 2015, 7.3, 219-242.

[13] Naveed Ul Haq, A., Nadhman, A., Ullah, I., Mustafa, G., Yasinzai, M., & Khan, I. "Synthesis approaches of zinc oxide nanoparticles: the dilemma of ecotoxicity." *Journal of Nanomaterials* 2017, 1, 8510342.

[14] Horie, Masanori, and Yosuke Tabei. "Role of oxidative stress in nanoparticles toxicity." *Free radical research*, 2021,5.44, 331-342.

[15] Miller, K. P., Wang, L., Benicewicz, B. C., & Decho, A. W., "*Inorganic nanoparticles engineered to attack bacteria."* Chemical Society Reviews, 2015, 44,21, 7787-7807.

[16] Permyakov, Eugene A., "*Metal binding proteins."* Encyclopedia, 2021, 1.1, 261-292.

[17] Bhattacharjee, N., Som, I., Saha, R., & Mondal, S., "*A critical review on novel eco-friendly green approach to synthesize zinc oxide nanoparticles for photocatalytic degradation of water pollutants."* International Journal of Environmental Analytical Chemistry, 2024, 104.3, 489-516.

[Downloaded from ijmse.iust.ac.ir on 2026-11-02]

[DOI: 10.22068/ijmse.4598]

in press

[18] Carrouel, F., Viennot, S., Ottolenghi, L., Gaillard, C., & Bourgeois, D., "*Nanoparticles as anti-microbial, anti-inflammatory, and remineralizing agents in oral care cosmetics" a review of the current situation.* Nanomaterials, 2020, 10.1,140.
[19] Osmond, M.J. and M.J. Mccall, "*Zinc oxide nanoparticles in modern sunscreens: an analysis of potential exposure and hazard."* Nanotoxicology, 2010, 4.1,15-41.
[20] Jamnongkan, T., Sukumaran, S. K., Sugimoto, M., Hara, T., Takatsuka, Y., & Koyama, K, "Towards novel wound dressings: Antibacterial properties of zinc oxide nanoparticles and electrospun fiber mats of zinc oxide nanoparticle/poly (vinyl alcohol) hybrids." *Journal of Polymer Engineering*, 2015, 35.6, 575-586.
[21] Espitia, P. J. P., C. G. Otoni, and N. F. F. Soares., "Zinc oxide nanoparticles for food packaging applications." *Antimicrobial food packaging*. Academic Press, 2025, 603-610.
[22] Siddiqi, K.S., "*Properties of zinc oxide nanoparticles and their activity against microbes.*" Nanoscale research letters, 2018, 13.1. 141.
[23] Ashraf, M. A., Peng, W., Zare, Y., & Rhee, K. Y., "Effects of size and aggregation/agglomeration of nanoparticles on the interfacial/interphase properties and tensile strength of polymer nanocomposites." *Nanoscale research letters*, 2018, 13.1, 214.
[24] Dong, Ya-nan, Li, X., Huang, Y., Wang, H., & Li, F., "Coagulation and dissolution of zinc oxide nanoparticles in the presence of humic acid under different pH values." *Environmental Engineering Science*, 2016, 33.5, 347-353.
[25] Bhong, Mahesh, Khan, T. K., Devade, K., Krishna, B. V., Sura, S., Eftikhaar, H. K., ... & Gupta, N., "Review of composite materials and applications." *Materials today: proceedings*, 2023.
[26] Abdulhussein, Huda J., Mohsin, M. H., Jabir, M. S., Sulaiman, G. M., Mohammed, H. A., Ismail, R. A., ... & Badher, N. S., "Eco-friendly synthesis of eggshell-derived nano-hydroxyapatite: physicochemical characterization, hemocompatibility, and bone regeneration potential." *Scientific Reports*, 2025, 15.1, 32832.
[27] Gupta, A., Prasad, A., Mulchandani, N., Shah, M., Ravi Sankar, M., Kumar, S., & Katiyar, V., "*Multifunctional nanohydroxyapatite-promoted toughened high-molecular-weight stereocomplex poly (lactic acid)-based bionanocomposite for both 3D-printed orthopedic implants and high-temperature engineering applications."* ACS omega, 2017, 2.7, 4039-4052.
[28] Khan, Idrees, Saeed, K., Ali, N., Zada, N., Khan, A., ... & Akhter, M. S., "Polymer nanocomposites: An overview." *Smart polymer nanocomposites*, 2023, 167-184.
[29] Causin, Valerio., "Polymers on the crime scene." *Polymers on the Crime Scene: Forensic Analysis of Polymeric Trace Evidence*. Cham: Springer International Publishing, 2015, 105-166.
[30] Behera, Manoranjan, and Shanker Ram., "*Inquiring the mechanism of formation, encapsulation, and stabilization of gold nanoparticles by poly (vinyl pyrrolidone) molecules in 1-butanol."* Applied Nanoscience, 2014, 4.2,247-254.
[31] Lee, Jim, Easteal, A. J., Pal, U., & Bhattacharyya, D., "Evolution of ZnO nanostructures in sol–gel synthesis." *Current Applied Physics.*, 2009, 9.4, 792-796.
[32] Hasnidawani, Azlina, H. N., Norita, H., Bonnia, N. N., Ratim, S., & Ali, E. S., "*Synthesis of ZnO nanostructures using sol-gel method."* Procedia chemistry, 2016, 19, 211-216.
[33] Boukhoubza, I., et al. "Morphological and structural properties of ZnO nanorods coated with graphene derivative fabricated by hydrothermal method." *Journal of Physics: Conference Series*. IOP Publishing , 2019, 1292.1, 012012.

[Downloaded from ijmse.iust.ac.ir on 2026-11-02]
[DOI: 10.22068/ijmse.4598]
In Press

[34] Kalpana, V., Kataru, B. A. S., Sravani, N., Vigneshwari, T., Panneerselvam, A., & Rajeswari, V. D., "*Biosynthesis of zinc oxide nanoparticles using culture filtrates of Aspergillus niger: Antimicrobial textiles and dye degradation studies."* OpenNano, 2018, 3, 48-55.

[35] Fouladi-Fard, R., Aali, R., Mohammadi-Aghdam, S., & Mortazavi-derazkola, S., "*The surface modification of spherical ZnO with Ag nanoparticles: A novel agent, biogenic synthesis, catalytic and antibacterial activities."* Arabian Journal of Chemistry, 2022, 15.3, 103658.

[36] Balogun, S.W., James, O. O., Sanusi, Y. K., & Olayinka, O. H., "*Green synthesis and characterization of zinc oxide nanoparticles using bashful (Mimosa pudica), leaf extract: a precursor for organic electronics applications."* SN Applied Sciences, 2020, 2.3, 504.

[37] Dai, F., Zhuang, Q., Huang, G., Deng, H., & Zhang, X., "*Infrared spectrum characteristics and quantification of OH groups in coal."* ACS omega, 2023, 8.19, 17064-17076.

[38] Mendes, C.R., Mendes, C. R., Dilarri, G., Forsan, C. F., Sapata, V. D. M. R., Lopes, P. R. M., de Moraes, P. B., ... & Bidoia, E. D., "*Antibacterial action and target mechanisms of zinc oxide nanoparticles against bacterial pathogens."* Scientific reports, 2022, 12.1, 2658.

[39] Shanavas, S., Priyadharsan, A., Karthikeyan, S., Dharmaboopathi, K., Ragavan, I., Vidya, C., ... & Anbarasana, P. M. "Green synthesis of titanium dioxide nanoparticles using Phyllanthus niruri leaf extract and study on its structural, optical and morphological properties." *Materials Today: Proceedings,* 2020,26, 3531-3534.

[40] Bureewong, Namthip, Injorhor, P., Krasaekun, S., Munchan, P., Waengdongbang, O., Wittayakun, J., ... & Ruksakulpiwat, Y.' "Preparation and Characterization of Acrylonitrile Butadiene Rubber Reinforced with Bio-Hydroxyapatite from Fish Scale." *Polymers*, 2023, 15.3, 729.

[41] Massoud, A., S. B. Challan, and Nabila Maziad. "Characterization of polyvinylpyrrolidone (PVP) with technetium-99m and its accumulation in mice." *Journal of Macromolecular Science,* 2021, *Part A* 58.6, 408-418.

[42] Batterjee, Maha G., Nabi, A., Kamli, M. R., Alzahrani, K. A., Danish, E. Y., & Malik, M. A., "Green hydrothermal synthesis of zinc oxide nanoparticles for UV-light-induced photocatalytic degradation of ciprofloxacin antibiotic in an aqueous environment." *Catalysts*, 2022, 12.11, 1347.

[43] Sharma, A., Singh, B. P., Dhar, S., Gondorf, A., & Spasova, M., "*Effect of surface groups on the luminescence property of ZnO nanoparticles synthesized by sol–gel route."* Surface Science, 2012. 606, 3-4, L13-L17.

[44] Vasconcellos, L. M. R. D., Nascimento, R. D., Cairo, C. A. A., Leite, D. D. O., Santos, E. L. D. S., Campos, G. E., ... & Carvalho, Y. R., "*Porous titanium associated with CaP coating: In vivo and in vitro osteogenic performance."* Materials Research, 2018. 21.2, e20170557.

[45] Singh, J., Kaur, S., Kaur, G., Basu, S., & Rawat, M., "Biogenic ZnO nanoparticles: A study of blueshift of optical band gap and photocatalytic degradation of reactive yellow 186 dye under direct sunlight." *Green Processing and Synthesis*, 2019, 8.1, 272-280.

[46] Ihsan, M., Din, I. U., Alam, K., Munir, I., Mohamed, H. I., & Khan, F., "*Green fabrication, characterization of zinc oxide nanoparticles using plant extract of Momordica charantia and Curcuma zedoaria and their antibacterial and antioxidant activities."* Applied biochemistry and biotechnology, 2023, 195.6, 3546-3565.

[Downloaded from ijmse.iust.ac.ir on 2026-11-02]

[DOI: 10.22068/ijmse.4598]

In Press

[47] Messih, M. A., Ahmed, M. A., Soltan, A., & Anis, S. S., "*Synthesis and characterization of novel Ag/ZnO nanoparticles for photocatalytic degradation of methylene blue under UV and solar irradiation."* Journal of Physics and Chemistry of Solids, 2019, 135, 109086.

[48] Fatimah, Purwiandono, G., Hidayat, H., Sagadevan, S., Ghazali, S. A. I. S. M., Oh, W. C., & Doong, R. A., "Flower-like SnO2 nanoparticle biofabrication using Pometia pinnata leaf extract and study on its photocatalytic and antibacterial activities." *Nanomaterials*, 2021, 11.11, 3012.

[49] Raghupathi, Krishna R., Ranjit T. Koodali, and Adhar C. Manna. "Size-dependent bacterial growth inhibition and mechanism of antibacterial activity of zinc oxide nanoparticles." *Langmuir*, 2011, 27.7, 4020-4028.

In Press

[Downloaded from ijmse.iust.ac.ir on 2026-11-02]

[DOI: 10.22068/ijmse.4598]